The Effect of Spatial and Temporal Wet-Troposphere Fluctuations on Connected Element Interferometry

C. D. Edwards
Tracking Systems and Applications Section

Numerical integrations of the structure function of tropospheric inhomogeneities have been performed to assess the impact of water vapor fluctuations on connected element interferometry (CEI). The expectation value of the RMS troposphere error for a differential spacecraft-quasar observation is derived by integrating the spatial refractivity structure function along raypaths to both the spacecraft and quasar from two spatially separated sites. Correlations between the tropospheric conditions at the two sites, which can become significant for short baseline observations, are fully accounted for in this calculation. Temporal effects are treated by assuming a frozen-flow model in which a fixed spatial distribution blows over both sites. Two "nominal" observation scenarios are considered, along with variations to study the dependence of the resultant differential troposphere errors on baseline length, observation time, source separation angle, and elevation. Consecutive differential observations are found to be almost completely uncorrelated, implying that averaging many repeated differential observations can quickly reduce the troposphere error.

I. Introduction

Uncalibrated signal delays due to propagation through the earth's atmosphere constitute one of the dominant error sources for Very Long Baseline Interferometry (VLBI). In particular, the delay component due to the wet troposphere is difficult to calibrate and can vary significantly both temporally and from site to site. For intercontinental measurements, the troposphere is typically modeled as a horizontally stratified distribution of water vapor, and a single parameter, the zenith wet troposphere delay, characterizes the troposphere at a given epoch and site. A mapping function (e.g., the Lanyi mapping function [1]) is used to determine the troposphere delay at other elevation angles. Surface meteorology can provide zenith wet troposphere calibrations with an accuracy of about 3 cm[1] [2], while water vapor radiometry offers the potential for 1-cm zenith calibrations [3].

[1] S. E. Robinson, "Errors in Surface Model Estimates of Zenith Wet Path Delays Near DSN Stations," JPL Interoffice Memorandum 335.4-594 (internal document), Jet Propulsion Laboratory, Pasadena, California, September 3, 1986.

In reality, the troposphere deviates significantly from this stratified model, because of spatial and temporal variations in the water vapor distribution. Tatarski [4] and Ishimaru [5] characterize spatial variations in the density of water vapor according to a power law structure function derived from Kolmogorov turbulence theory. Treuhaft and Lanyi [6, 7] have performed numerical integrations of this power law to derive a spatial structure function

$$D_{\tau,\theta,\phi}(\boldsymbol{\rho}) = \langle(\tau_{\theta,\phi}(\mathbf{x}+\boldsymbol{\rho}) - \tau_{\theta,\phi}(\mathbf{x}))^2\rangle \qquad (1)$$

where $\tau_{\theta,\phi}(\mathbf{x})$ is the wet tropospheric delay, observed from position $\mathbf{x}$ at elevation θ and azimuth ϕ relative to the baseline vector $\boldsymbol{\rho}$. To the extent that the wet troposphere can be modeled as a fixed spatial distribution of water vapor blowing over a site, this spatial structure function can also be used to describe temporal variations at a single site by replacing the baseline vector $\boldsymbol{\rho}$ with the product of windspeed $\mathbf{v}$ and time t [5–7].

Using the DSN Block 0 VLBI dataset, Treuhaft and Lanyi [6, 7] have shown that these temporal variations are a dominant error source for the VLBI phase-rate observable. On the other hand, given Block 0 system noise contributions, the delay-observable error for intercontinental VLBI is dominated more by overall zenith delay uncertainty than by the small-scale spatial and temporal fluctuations at each site. Certain observation scenarios, however, can lead to a significant reduction in the error component due to the zenith uncertainty and thereby increase the relative importance of the stochastic troposphere errors. For Delta-Differenced One-way Range (ΔDOR) observations, in which delay measurements are made for a pair of angularly close radio sources (typically a spacecraft and a quasar), significant cancellation is obtained in the tropospheric delay error due to the proximity of the raypaths at each site. In addition, for short baseline observations, the troposphere delays over the two stations become highly correlated. In both these scenarios, the troposphere delay error due to zenith delay uncertainty in the context of a stratified troposphere model is greatly reduced. A proper understanding of the delay error budget requires a careful treatment of the spatial and temporal troposphere inhomogeneities.

In this article, both these sources of correlation are considered. Numerical integrations are performed to calculate the size of delay errors for differential delay observations of a pair of radio sources on short baselines. The motivation for this analysis is a desire to quantify the impact of the wet troposphere on differential spacecraft-quasar CEI navigation measurements and to explore the dependence of the troposphere error on observation parameters such as baseline length, time difference between observations, source-pair separation angle, and elevation angle. These results should also be of interest for GPS applications; in particular, the calculations reported here are relevant to the proper weighting of spacecraft-differenced range data on small-scale regional networks.

For CEI, it is crucial to understand the delay error budget at the millimeter level, since a 1-mm delay error on a 20-km baseline represents a 50-nrad angular error. (To put this in perspective, Block I VLBI on intercontinental baselines will deliver roughly 50-nrad angular accuracy for the upcoming Galileo mission.[2]) This article refers to the CEI differential delay measurement as ΔDOΦ to emphasize that the observable is based on the highly precise phase-delay datatype. Existing Block 0 VLBI observations on the DSS-12–DSS-13 and DSS-13–OVRO baselines have already demonstrated phase-delay precision (based on quasar SNR) of under 1 psec, with residual scatter for angularly close sources on the order of 10 psec [8, 9].

The analysis reported here constitutes a straightforward extension of the work of Treuhaft and Lanyi [6, 7]. Whereas their structure function $D_{\tau,\theta,\phi}(\boldsymbol{\rho})$ represents the expected variance of the troposphere delay along two lines of sight, separated by a distance $\boldsymbol{\rho}$, the calculations here will involve four lines of sight, one at each station for each of the two radio sources. All correlations among the fluctuations on these four raypaths are accounted for in this analysis.

II. Derivation of the ΔDOΦ Troposphere Error

Let $\tau_{\Delta DO\Phi}$ be the troposphere-induced differential phase-delay error:

$$\tau_{\Delta DO\Phi} = [\tau_{\theta_A,\phi_A}(\boldsymbol{\rho}) - \tau_{\theta_A,\phi_A}(\mathbf{0})] - [\tau_{\theta_B,\phi_B}(\boldsymbol{\rho} - \mathbf{v}\,\delta t) - \tau_{\theta_B,\phi_B}(-\mathbf{v}\,\delta t)] \qquad (2)$$

Each τ represents the troposphere delay along a certain line-of-sight. The indices A and B refer to the two radio sources, $\boldsymbol{\rho}$ is the vector between the two sites, $\mathbf{v}$ is the wind velocity, and δt is the time between observations of A and B. The first two

[2] J. B. Thomas, "An Error Analysis for Galileo Angular Position Measurements with the Block I ΔDOR System," JPL Engineering Memorandum 335-26 (internal document), Jet Propulsion Laboratory, Pasadena, California, November 11, 1981.

terms represent the differential troposphere between the two stations (at positions **0** and $\boldsymbol{\rho}$) for the observation of source A, while the second two terms represent the differential troposphere observed at time δt later for the observation of source B.

Following the approach of Treuhaft and Lanyi [6, 7], each of the four path delays in this formula can be expressed as an integration of the refractivity $\chi(\mathbf{r})$ along the given raypath:

$$\tau_{\theta_A,\phi_A}(\mathbf{x}) = \frac{1}{\sin\theta_A}\int_0^h dz\,\chi(\mathbf{x} + \mathbf{r}(\theta_A,\phi_A,z)) \tag{3}$$

where $\mathbf{r}$ ranges along the θ_A,ϕ_A line-of-sight, and where the raypath integration has been truncated at height h. One assumes that $\langle\chi(\mathbf{r})\rangle$ and $\langle\chi^2(\mathbf{r})\rangle$ are independent of $\mathbf{r}$. Also, throughout this analysis, one assumes a flat earth, and hence the azimuths and elevations at the two stations will be the same for any given source. For baseline lengths of tens or even a few hundreds of km, this is a reasonable approximation.

Substituting the delay path integrals of Eq. (3) into Eq. (2), one obtains

$$\begin{aligned}\langle\tau^2_{\Delta DO\Phi}\rangle = \Bigg\langle\Bigg\{&\frac{1}{\sin\theta_A}\int_0^h dz\,\chi(\boldsymbol{\rho} + \mathbf{r}(\theta_A,\phi_A,z)) \\ &- \frac{1}{\sin\theta_A}\int_0^h dz\,\chi(\mathbf{r}(\theta_A,\phi_A,z)) \\ &- \frac{1}{\sin\theta_B}\int_0^h dz\,\chi(\boldsymbol{\rho} - \mathbf{v}\delta t + \mathbf{r}(\theta_B,\phi_B,z')) \\ &+ \frac{1}{\sin\theta_B}\int_0^h dz\,\chi(-\mathbf{v}\delta t + \mathbf{r}(\theta_B,\phi_B,z'))\Bigg\}^2\Bigg\rangle\end{aligned} \tag{4}$$

By expanding this expression, interchanging the order of averaging and integration, and making use of the relation

$$D_\chi(|\mathbf{x}_1 - \mathbf{x}_2|) = 2\langle\chi^2\rangle - 2\langle\chi(\mathbf{x}_1)\chi(\mathbf{x}_2)\rangle \tag{5}$$

the delay error is obtained as a double integral of a sum of refractivity structure functions:

$$\begin{aligned}\langle\tau^2_{\Delta DO\Phi}\rangle = \int_0^h\int_0^h dz dz' \Bigg\{&-\frac{1}{\sin^2\theta_A} D_\chi(|\mathbf{r}(\theta_A,\phi_A,z) - \mathbf{r}(\theta_A,\phi_A,z')|) \\ &- \frac{1}{\sin^2\theta_B} D_\chi(|\mathbf{r}(\theta_B,\phi_B,z) - \mathbf{r}(\theta_B,\phi_B,z')|) \\ &+ \frac{1}{\sin^2\theta_A} D_\chi(|\boldsymbol{\rho} + \mathbf{r}(\theta_A,\phi_A,z) - \mathbf{r}(\theta_A,\phi_A,z')|) \\ &+ \frac{1}{\sin^2\theta_B} D_\chi(|\boldsymbol{\rho} + \mathbf{r}(\theta_A,\phi_A,z) - \mathbf{r}(\theta_B,\phi_B,z')|) \\ &+ \frac{2}{\sin\theta_A\sin\theta_B} D_\chi(|\mathbf{r}(\theta_A,\phi_A,z) + \mathbf{v}\delta t - \mathbf{r}(\theta_B,\phi_B,z')|) \\ &- \frac{1}{\sin\theta_A\sin\theta_B} D_\chi(|\boldsymbol{\rho} + \mathbf{r}(\theta_A,\phi_A,z) + \mathbf{v}\delta t - \mathbf{r}(\theta_B,\phi_B,z')|) \\ &- \frac{1}{\sin\theta_A\sin\theta_B} D_\chi(|\mathbf{r}(\theta_A,\phi_A,z) - \boldsymbol{\rho} + \mathbf{v}\delta t - \mathbf{r}(\theta_B,\phi_B,z')|)\Bigg\}\end{aligned} \tag{6}$$

Using the Kolmogorov expression for $D_\chi(r)$

$$D_\chi(r) = \langle(\chi(\mathbf{r}) - \chi(\mathbf{0}))^2\rangle = C^2 r^{2/3} \quad (7)$$

Eq. (6) can be numerically integrated to estimate $\tau^2_{\Delta DO\Phi}$ as a function of ρ, δt, θ_A, ϕ_A, θ_B, and ϕ_B. C is a scale factor that characterizes the amplitude of refractivity fluctuations.

III. Numerical Integration Results

The double integration in Eq. (6) was evaluated numerically, using the same values for the three free parameters h, v, and C as were used by Treuhaft and Lanyi [6, 7]: the effective troposphere height h was taken as 1 km, the wind speed v_{wind} was set at 8 m/sec, and a fluctuation amplitude C of 2.4×10^{-7} $m^{-1/3}$ was adopted. These results yield a normalization consistent with observed VLBI, WVR, and radiosonde data from the three DSN complexes.

Each $\Delta DO\Phi$ observation was specified by the following parameters:

- θ_0, ϕ_0 = the arithmetic mean of the elevation and azimuth angles of the two sources A and B
- δs = the separation angle (arclength) between the two radio sources; the separation can be solely in azimuth (equal elevation angles) or in elevation (equal azimuths)
- L = the baseline length between the two CEI stations (the baseline azimuth is fixed at 0)
- δt = the time separation between the two observations
- ϕ_{wind} = the wind azimuth

For this analysis, a "nominal" configuration was considered, with θ_0 = 45 deg and ϕ_0 = 60 deg. The baseline length L was set to 21 km, corresponding to the length of the DSS-13–DSS-14 and DSS-13–DSS-15 baselines at Goldstone, while the 8-m/sec wind was directed at an azimuth ϕ_{wind} = −60 deg. A separation angle of 10 deg was adopted for δs, with a time separation δt of 200 sec. Two cases were considered: the AZ case, for which the angular source separation was solely azimuthal, and the EL case, for which the sources were separated solely in elevation. The configurations are summarized in Table 1.

The nominal configuration yielded an RMS $\Delta DO\Phi$ troposphere error of 4.52 mm for the AZ case and 4.56 mm for the EL case. To study the dependence of these errors on the observation scenario, the configuration parameters were varied one at a time over a range of values, and the $\Delta DO\Phi$ troposphere error calculated as a function of that parameter. Four parameters were allowed to vary: the baseline length L, the time δt between observations, the mean elevation angle θ_0, and the separation angle δs. Figures 1–4 show the results of varying each of these parameters about the nominal configurations.

A. Baseline Length Dependence

Figure 1 shows the calculated RMS $\Delta DO\Phi$ troposphere error

$$\sigma_{\Delta DO\Phi} \equiv \sqrt{\langle \tau^2_{\Delta DO\Phi} \rangle} \quad (8)$$

as the baseline length L is allowed to vary from 1 km up to 1000 km, and all other parameters are held at their nominal values. The solid and dashed lines indicate the results for varying the AZ and EL configurations, respectively. For azimuthal source separation, very little dependence on baseline length is observed: $\sigma_{\Delta DO\Phi}$ is nearly saturated even at the nominal 21-km baseline length, and drops only to 3.1 mm when the baseline length is reduced to 1 km. For source separation in the elevation direction, $\sigma_{\Delta DO\Phi}$ again varies quite slowly for baseline lengths of under 100 km, but it does not saturate as in the AZ case; rather, $\sigma_{\Delta DO\Phi}$ continues to grow as L increases to 1000 km. This can be understood intuitively by returning to the stratified troposphere model in which the troposphere is fully characterized by a zenith value. For the EL configuration, the A and B sources are at different elevation angles and hence have different zenith mapping functions. Thus the EL case is sensitive to the zenith path-delay difference between the two sites, which tends to grow with baseline length. For the AZ case, the elevation angles of A and B are identical, and so any zenith delay difference is canceled.

Based on the slow L dependence observed in these plots, one is driven towards longer baselines, subject to the constraint, of course, that phase ambiguities can be reliably resolved. Since the troposphere delay error grows much slower than baseline length, the angular error $\sigma_{\Delta DO\Phi}/L$ will decrease rapidly with increasing baseline. For instance, increasing the baseline length from the nominal value of 21 km up to 200 km leads to less than a 20 percent increase in the troposphere error for the EL case (and nearly no increase at all for the AZ case), translating into better than an eight-fold improvement in angular accuracy.

B. Observation Time Dependence

In Fig. 2, one sees the effect of varying δt over the range from 10 sec to 10,000 sec. The observed dependence on δt is much stronger than for the baseline length. In the neighborhood of the nominal value of δt = 200 sec, the dependence is

fairly strong. For instance, for the EL case, reducing δt to 60 sec would lower $\sigma_{\Delta DO\Phi}$ to 2.6 mm, a reduction of over 40 percent. The AZ and EL cases look quite similar, with the most significant difference being a slightly lower $\sigma_{\Delta DO\Phi}$ for the AZ case at very short differential observation times.

This result suggests that minimizing the time separation of differential observations should be an important design goal for a CEI navigation system. In particular, maximum safe slew rates should be used, and observation times should be kept as short as possible while still providing sufficient SNR to keep the inherent data noise at or below the level of the troposphere. The wide bandwidth offered by fiber optics provides one means of reducing observation times. The current Block 0 system, with which existing phase-delay data have been obtained [8, 9], offers a 2-MHz observation bandwidth. Low-noise HEMT amplifiers and single-mode fibers can support bandwidths of several hundred MHz, leading to over an order of magnitude decrease in observation time for comparable SNR.

It should be pointed out that the calculations here are for a pair of instantaneous observations, separated by a time δt. For observations of finite length, δt would represent the time difference between the midpoints of each scan, i.e., half the scan time for source A plus half the scan time for source B plus the slew time in-between scans. A more accurate treatment would account for the averaging of the troposphere over a scan. In other words, for a scan length of T_s, the tropospheric path delay $\tau_{\theta_A,\phi_A}(\mathbf{x})$ should be replaced by a mean path delay over the length of the scan as follows:

$$\bar{\tau}_{\theta_A,\phi_A}(\mathbf{x},T_s) = \frac{1}{T_s}\int_{-T_s/2}^{T_s/2} dt\, \tau_{\theta_A,\phi_A}(\mathbf{x}-\mathbf{v}t) \tag{9}$$

This averaging, by effectively acting as a low-pass filter on the troposphere with a cutoff frequency $\nu_c \approx 1/T_s$, will tend to reduce $\sigma_{\Delta DO\Phi}$ somewhat, particularly when the scan length T_s is a large fraction of the time difference δt between scan midpoints.

To quantify the size of this effect, such a calculation is carried out for the two nominal configurations, with a scan length T_s of 60 sec, and approximating the integral in Eq. (9) by dividing the scan into five sections:

$$\bar{\tau}_{\theta_A,\phi_A}(\mathbf{x},T_s) = \frac{1}{5}\sum_{i=1}^{5}\tau_{\theta_A,\phi_A}(\mathbf{x}-\mathbf{v}t_i) \tag{10}$$

where $t_i = \{-24, -12, 0, +12, +24\}$ sec for $i = \{1, \ldots, 5\}$. Substituting these mean path delays into Eq. (2) yields an expression for $\tau_{\Delta DO\Phi}$ involving twenty separate raypaths. And when this is squared to evaluate $\langle\tau^2_{\Delta DO\Phi}\rangle$, there are four-hundred cross-terms, posing a significantly larger computational task. A modification of the original program was made to evaluate this finite-length scan version of the $\Delta DO\Phi$ error. For the nominal EL configuration, the value of $\sigma_{\Delta DO\Phi}$ decreased only slightly to 4.42 mm, a change of only 3 percent. A similar reduction of about 3 percent was also obtained for the AZ case. Given the small size of these corrections, the assumption of instantaneous scans should not seriously affect the conclusions of this analysis. (Further subdividing the scans into more than five sections did not lead to any additional significant reductions, verifying that the summation in Eq. (10) is an adequate approximation of the integral in Eq. (9).)

C. Elevation Angle Dependence

Figure 3 shows the effect of varying the mean elevation angle of the two sources, while holding their angular arclength separation constant. For source separations in either the azimuth or elevation direction, the $\Delta DO\Phi$ troposphere error rises sharply for elevation angles below 30 deg. At these low elevations, the atmospheric pathlength of roughly $1/\sin(\theta)$ increases rapidly with decreasing elevation, with a consequent increase in the size of path delay variations. One distinct advantage of the shorter baselines used in CEI is that sources can be observed at much higher elevation angles. For a Goldstone CEI system, with latitude +35 deg, a source at zero declination has an elevation of 55 deg at transit. The ecliptic plane, in which most DSN missions take place, is inclined 23 deg with respect to the earth's polar axis, and so the ecliptic ranges from +23 deg to −23 deg declination. A source at +23 deg declination would transit at 78 deg elevation, while a source at −23 deg declination would transit at 32 deg elevation. Thus even an ecliptic plane source at extreme southern declinations could be observed from Goldstone at reasonable elevations. Nonetheless, southern declination observations from Goldstone can be expected to be of poorer resolution, given these lower elevation angles. As a result, optimal CEI tracking throughout the ecliptic may warrant a second CEI site in the southern hemisphere.

D. Angular Source Separation Dependence

Finally, in Fig. 4, the separation angle δs is varied, while the mean values of the azimuth and elevation angles for the two sources are kept fixed. For the AZ case, with both sources at the same elevation angle, $\sigma_{\Delta DO\Phi}$ is nearly independent of δs. For the EL case, $\sigma_{\Delta DO\Phi}$ varies slowly for separation angles δs less than 20 deg, but begins to rise sharply for δs above 40 deg.

To understand this, it is necessary to consider the various distance scales in the CEI observing geometry. The observation time scale of $\delta t = 200$ sec corresponds to a distance scale of $v_{wind} \times \delta t = 1.6$ km. At each site, there is another distance scale corresponding to the spatial separation of the two raypaths, which can be characterized by the distance r between the two raypaths at the effective troposphere height h. This distance r can be expressed

$$r = h\sqrt{\cot^2\theta_A + \cot^2\theta_B - 2\cot\theta_A \cot\theta_B \cos(\phi_A - \phi_B)} \tag{11}$$

For the AZ case of $\theta_A = \theta_B = 45$ deg, $r = 2\sqrt{1 - \cos(\delta s)}$ which even for $\delta s = 60$ deg is 1.4 km. Thus, for the AZ case, the temporal errors associated with the difference between observations dominate the spatial errors due to source separation, at least for $\delta s < 60$ deg.

For the EL case, $\phi_A = \phi_B$, and so the effective raypath spatial separation is

$$r = |\cot\theta_A - \cot\theta_B| \tag{12}$$

which is 1.7 km for a δs of 40 deg, comparable to the 200 sec scale, and which rises to $r = 3.5$ km at $\delta s = 60$ deg. Thus for large elevation separations, the spatial scale begins to dominate over the temporal scale above $\delta s = 40$ deg. Here again is visible the complex interplay of the various distance scales involved in the CEI observing geometry.

The slow variation of $\sigma_{\Delta DO\Phi}$ with δs over the range of 0–20 deg means that for CEI observations it may be more profitable to use a strong quasar 20 deg from the spacecraft, rather than a weaker quasar within 5 deg. The stronger quasar would require a shorter scan length, thereby reducing the more dominant temporal troposphere variation. Of course, other error sources, such as gravity-induced antenna deformations, may argue for keeping source separation as small as possible.

IV. Discussion

These calculations should help in the system design of a dedicated CEI facility at Goldstone and should also serve as a tool for optimizing observations using such a system. It is important to remember, however, that the results obtained are dependent on the input parameters C, h, and v_{wind}. Changing C will only change the overall normalization of the $\Delta DO\Phi$ error, but h and v_{wind} are two of the fundamental scales in the CEI $\Delta DO\Phi$ geometry; changing them will affect the shape of the functional dependence of $\sigma_{\Delta DO\Phi}$ on L, δt, θ_0, and δs. It is likely that C, h, and v_{wind} change on a daily basis, and one important task would be to collect statistics on these parameters by fitting single-site temporal structure functions, perhaps using water vapor radiometers or spectral hygrometers as a source of data.

The results presented here represent the expected wet troposphere error for a single $\Delta DO\Phi$ error, with no external troposphere calibrations. A number of different techniques could provide further means for achieving significant reductions in the $\Delta DO\Phi$ troposphere error. For instance, water vapor radiometers may have the potential to supply differential line-of-sight path-delay calibrations at the millimeter level. Whereas overall zenith troposphere calibration requires highly accurate WVR gain calibrations, differential line-of-sight WVR calibrations place more stringent demands on the temporal stability of the WVR, and on accurate modeling of the WVR beam. Studies are under way to determine the short-term noise floor of current WVRs, and to quantify their utility for differential delay and delay rate calibrations. A 1-mm calibration capability could significantly reduce $\Delta DO\Phi$ troposphere errors, based on the expected level of fluctuations calculated here.

A second approach to reducing troposphere errors is to simply average many repeated $\Delta DO\Phi$ observations. Since the wet troposphere fluctuations are stochastic in nature, the troposphere error on the mean of many observations will be less than the error on each individual observation. Of course, additional observations will help only to the extent that they are uncorrelated from previous observations. The correlation between successive $\Delta DO\Phi$ observations is expressed analytically as

$$\rho(T_{sep}) = \frac{\left\langle \tau_{\Delta DO\Phi}(t=0)\tau_{\Delta DO\Phi}(t=T_{sep}) \right\rangle}{\sigma^2_{\Delta DO\Phi}} \tag{13}$$

where T_{sep} is the time separation between the two $\Delta DO\Phi$ observations (expressed as the difference between the epochs of the midpoints of the individual $\Delta DO\Phi$ observations). The denominator is the tropospheric delay variance for the individual $\Delta DO\Phi$ observations, while the numerator can be expanded as

$$\Big\langle ([\tau_A(\boldsymbol{\rho}) - \tau_A(\mathbf{0})] - [\tau_B(\boldsymbol{\rho} - \mathrm{v}\,\delta t) - \tau_B(-\mathrm{v}\,\delta t)]) \times ([\tau_A(\boldsymbol{\rho} - \mathrm{v}T_{sep}) - \tau_A(-\mathrm{v}T_{sep})] - [\tau_B(\boldsymbol{\rho} - \mathrm{v}\,\delta t - \mathrm{v}T_{sep}) - \tau_B(-\mathrm{v}\,\delta t - \mathrm{v}T_{sep}]) \Big\rangle \quad (14)$$

where δt is, as in Eq. (2), the separation between the A and B sources within a single ΔDOΦ observation. (The subscripts A and B implicitly refer to the source directions (θ_A, ϕ_A) and (θ_B, ϕ_B).)

Figure 5 shows the results of evaluating $\rho(T_{sep})$ numerically for both the AZ and EL configurations. The calculation is similar to the calculation of $\sigma_{\Delta DO\Phi}$ in Section II, but with eight rather than four separate raypaths to consider. The time separation δt for the individual ΔDOΦ observations was held fixed at 200 sec, and T_{sep} was allowed to vary from 10 sec up to 10^4 sec. (Note that for $T_{sep} < \delta t$, the two ΔDOΦ observations actually overlap.) For both the AZ and EL configurations, $\rho(T_{sep})$ drops very quickly as T_{sep} increases. By the time T_{sep} has reached 200 sec, corresponding to back-to-back ΔDOΦ observations with no idle time, $\rho(T_{sep})$ has dropped to well below 10 percent. In other words, at least for the geometry considered here, ΔDOΦ observations could be conducted continuously, and the troposphere errors $\sigma_{\Delta DO\Phi}$ for adjacent observations would be almost entirely uncorrelated. This important conclusion means that the ΔDOΦ troposphere error can be rapidly reduced to the millimeter level through statistical averaging of many consecutive observations.

Another technique which could further reduce CEI troposphere errors would be to apply the Local Reference Frame concept in which several quasar sources are observed along with the spacecraft. For intercontinental VLBI, a covariance study has shown [10] that referencing the spacecraft position to several spatially distributed quasars (instead of a single quasar as in traditional ΔDOR), enables dominant systematic error sources to be removed through parameter estimation. Although the ΔDOΦ error budget is quite different, a similar technique might enable improved accuracy for short baselines. With quasars distributed spatially around the spacecraft, particularly over a range of elevation angles, it should be possible to filter out some of the large scale troposphere inhomogeneities which limit the ΔDOΦ observable. This is another interesting area for future work.

One point which should be clear is that it is difficult to intuitively estimate the troposphere error for a specific geometry, given the complex interplay of the various spatial and temporal dimensions. To obtain meaningful error estimates for differential observations on short baselines, it is essential to account for the statistics of wet troposphere fluctuations. It is hoped that future CEI covariance analyses and data reduction algorithms will incorporate these results.

V. Conclusions

CEI ΔDOΦ observations achieve a high degree of double-differential troposphere cancellation due to the proximity of the stations and the small angular separation of the sources. Fluctuations along the four ΔDOΦ raypaths are likely to be a dominant error source for CEI ΔDOΦ navigation. The CEI ΔDOΦ geometry contains many different distance scales, complicating any simple intuitive models. To quantify the effects of these fluctuations for an arbitrary observing geometry, an expression has been derived for the troposphere error $\sigma_{\Delta DO\Phi}$ expressed as a double integral of the refractivity structure function, similar to the single station or single source expressions derived by Treuhaft and Lanyi [6, 7], but accounting for all correlations among the four ΔDOΦ raypaths.

For a nominal observation scenario, this double integral has been evaluated numerically, yielding troposphere-induced ΔDOΦ errors of about 4.5 mm for 10-deg source separations, with a very slow dependence on baseline length. A much stronger dependence is observed for variations of the time difference between the A and B observations. For this nominal observation, $\sigma_{\Delta DO\Phi}$ can be reduced over 40 percent by lowering δt from 200 sec to 60 sec. Observations below 20 deg appear to be significantly degraded due to the rapidly increasing pathlength and resultant increased amplitude of fluctuations. For the nominal configuration, varying the angular source separation from 0 to 20 deg produced a very slow increase in $\sigma_{\Delta DO\Phi}$. However, as the source separation was increased beyond 40 deg in elevation, $\sigma_{\Delta DO\Phi}$ increased rapidly. Finally, the correlation between repeated ΔDOΦ observations was calculated and found to be quite small, indicating that the troposphere fluctuation errors can be quickly reduced through averaging many repeated observations.

Acknowledgments

I would like to thank Gabor Lanyi and Bob Treuhaft for helpful discussions regarding the troposphere structure function, and Mark Finger for suggesting a technique for converting the two-dimensional troposphere integrals into more efficient one-dimensional integrals using Gauss's Law.

References

[1] G. E. Lanyi, "Tropospheric Delay Effects in Radio Interferometry," *TDA Progress Report 42-78*, vol. April–June 1984, Jet Propulsion Laboratory, Pasadena, California, pp. 152–159, August 15, 1984.

[2] C. C. Chao, "The Tropospheric Calibration Model for Mariner Mars 1971," NASA–JPL Technical Report TR-32-1587, Jet Propulsion Laboratory, Pasadena, California, pp. 61–76, 1974.

[3] S. E. Robinson, "The Profile Algorithm for Microwave Delay Estimation from Water Vapor Radiometer Data," *Radio Sci.*, vol. 23, pp. 401–408, 1988.

[4] V. I. Tatarski, *Wave Propagation in a Turbulent Medium*, New York: Dover, 1961.

[5] A. Ishimaru, *Wave Propagation and Scattering in Random Media*, New York: Academic Press, 1978.

[6] R. N. Treuhaft and G. E. Lanyi, "The Effect of the Dynamic Wet Troposphere on Radio Interferometric Measurements," *Radio Sci.*, vol. 22, pp. 251–265, 1987.

[7] R. N. Treuhaft and G. E. Lanyi, "The Effect of the Dynamic Wet Troposphere on VLBI Measurements," *TDA Progress Report 42-84*, vol. October–December 1985, Jet Propulsion Laboratory, Pasadena, California, pp. 1–17, February 15, 1986.

[8] C. Edwards, "Short Baseline Phase Delay Interferometry," *TDA Progress Report 42-91*, vol. July–September 1987, Jet Propulsion Laboratory, Pasadena, California, pp. 46–56, November 15, 1987.

[9] C. Edwards, "Angular Navigation Capabilities of Short Baseline Phase Delay Interferometry," Paper 88-4287, AIAA/AAS Astrodynamics Conference, Minneapolis, Minnesota, August 15–17, 1988.

[10] R. Treuhaft, "Few-Nanoradian Deep Space Navigation in Local Reference Frames," Paper 88-4288, AIAA/AAS Astrodynamics Conference, Minneapolis, Minnesota, August 15–17, 1988.

Table 1. Nominal observation configurations

Parameter	Measurement
θ_0	45 deg
ϕ_0	60 deg
δs	10 deg (either AZ or EL)
L	21 km
δt	200 sec
v_{wind}	8 m/sec
ϕ_{wind}	-60 deg
h	1 km
C	2.4×10^{-7} $m^{-1/3}$

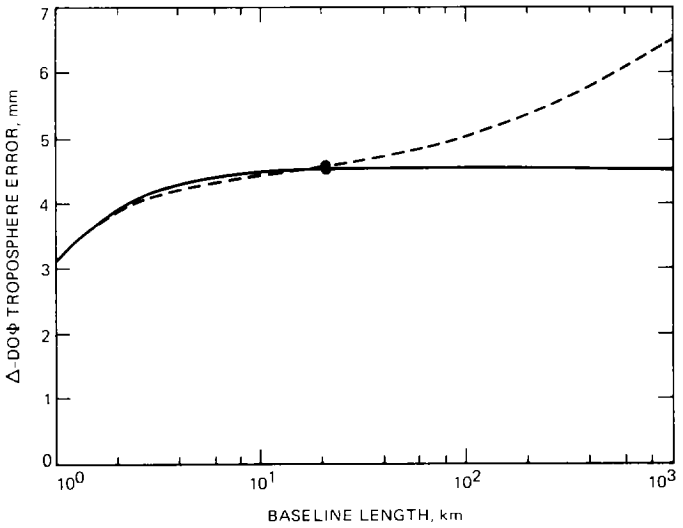

Fig. 1. Dependence of the ΔDOΦ troposphere error on baseline length. For all plots, the solid line represents the AZ configuration (sources separated in azimuth) while the dashed line represents the EL configuration (sources separated in elevation.) For Figs. 1–4, the dot on each curve indicates the nominal AZ or EL configuration.

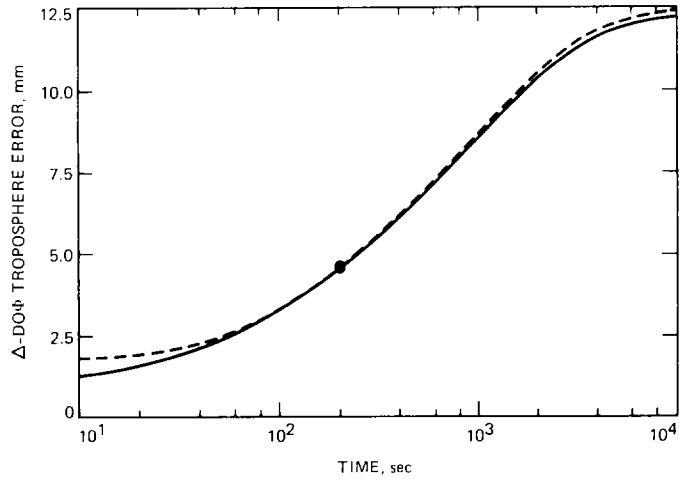

Fig. 2. Dependence of the ΔDOΦ troposphere error on the time separation between observations.

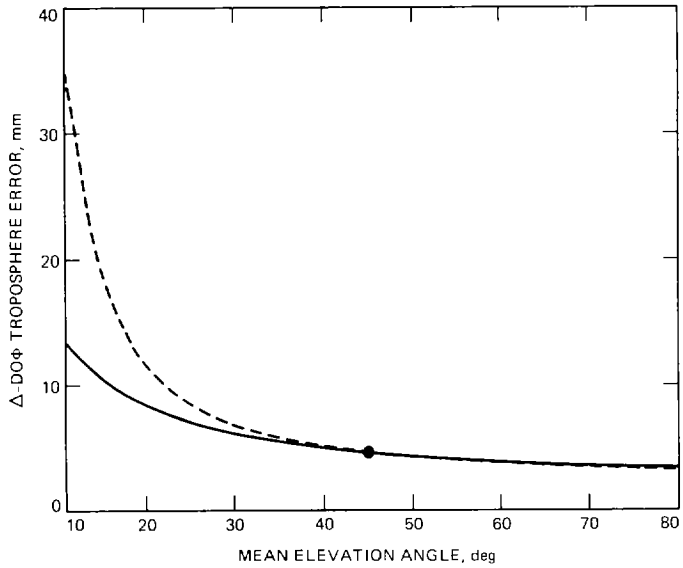

Fig. 3. Dependence of the ΔDOΦ troposphere error on the mean elevation angle of the source pair. The separation arclength is held fixed as the mean elevation is varied.

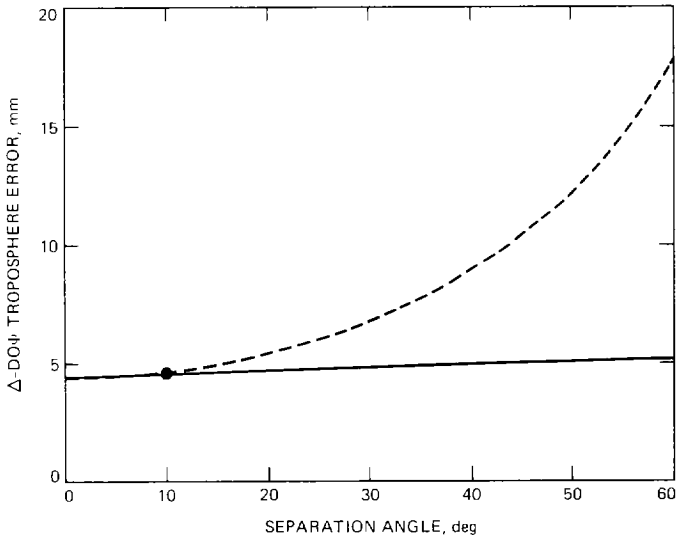

Fig. 4. Dependence of the ΔDOΦ troposphere error on the separation angle of the source pair. The mean elevation angle is held fixed as the separation angle is varied.

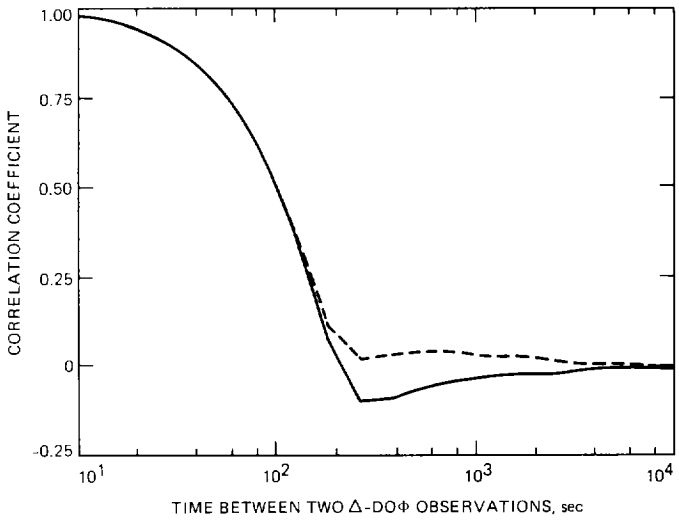

Fig. 5. Correlation between two successive ΔDOΦ observations. The X-axis represents the time separation T_{sep} between the midpoints of the two ΔDOΦ measurements. For each ΔDOΦ observation, the observations of the *A* and *B* sources are separated by a time δt = 200 sec. So, for T_{sep} < 200 sec, the two ΔDOΦ measurements actually overlap. Note that the correlation drops very quickly: consecutive non-overlapping ΔDOΦ measurements are almost completely uncorrelated, indicating that statistical averaging can be used to reduce the size of the troposphere errors through repeated measurements.